Intelligent Real-time Power Management of Multi-Source HEVs based on Driving State Recognition and Offline Optimization

Ahmed M. Ali, *Member, IEEE* Bedatri Moulik, and Dirk Söffker, *Member, IEEE*

***Abstract*—Electric vehicles (EVs) are promising alternatives to carbonized propulsion-based vehicles. They are capable of reducing environmental degradation without compromising driving performance. Power management strategies (PMS) are particularly essential for electrified vehicles to ensure optimal power split between on-board energy storage sources and to meet operational requirements of each source. However, optimization concept in PMS, have been constantly addressed in literature to achieve optimal power handling decisions in real-time, particularly under unknown driving conditions. In this contribution, an intelligent rule-based PMS with embedded offline-optimized control parameters and online driving state recognition is proposed to achieve optimal power handling decisions for EVs situatively and adaptively. A set of characteristic variables defining driving states have been extracted from representative segments of several driving cycles, to which optimized control strategies are tuned offline. Three different driving cycles representing urban, highway, and mixed trip conditions have been implemented for comparative investigation of achieved results. The analysis of results reveals the potential of proposed PMS to reduce the energy consumption by 13.6 – 30.9 %.**

***Index Terms*—hybrid electric vehicles, adaptive power management, drive pattern recognition**

I. INTRODUCTION

REDUCTION of carbon footprint and mitigation of fossil fuel depletion is considered as a global concern in transportation technology. Electrified powertrains are promising alternatives to fossil fuel–empowered vehicles in terms of extended mileage, higher fuel economy, and lower emission rates. Power management of electric vehicles (EVs) is an important development tool considering variable power demand and trip conditions. In this context, solution optimality and real-time applicability are essential requirements for evaluating PMS algorithms. While many sophisticated methods were capable of finding a global optimum with respect to relevant conflicting criteria, real-time applicability of such methods is limited. The need for an applicable algorithm, yet capable to provide near-optimal solutions is non-trivial challenge for vehicular control schemes [1].

Fuel cell vehicles (FCVs) has been receiving particular attention, as clean and efficient propulsion systems. However, FCVs are typically hybridized with other energy sources, i.e. battery and supercapacitors, to count for the inferior power density of fuel cells [2]. The synergy role of the supercapacitor is to act as a power buffer when the load demand peaks at high transients and hence, to allow the battery to operate at nearly steady-state conditions. This prevents the battery from suffering pre-matured aging and damage. PMS of FCVs play a significant role in defining optimal power handling strategies to reduce energy consumption and fulfill driveability requirements [3].

Existing PMS can be categorized into rule-based and optimization-based algorithms. Optimization-based algorithms are formulated to find an optimal power management strategy for a specific driving cycle, given a priori. The computational complexity of such algorithms lacks its real-time applicability on vehicular controllers. On the other side, rule-based algorithms are widely implemented as they are computationally efficient. However, rules definition in such methods is generally based on human experience and therefore, optimal performance is not guaranteed [4].

The overview of literature gives an insight that addressing main deficiencies of rule-based PMS has been receiving an increasing attention in the last few years. Improvement of solution optimality and preserving real-time applicability of such algorithms has been the focus of many recent advances in PMS [5]. A comprehensive analysis of previous works is presented in the sequel, to point out relevant contributions and which to put forward the potential of optimized rule-based PMS to address the main challenges of EVs.

A. Literature review

Inferior optimality of rule-based solutions has been tackled in literature using two main approaches: offline rules optimization and development of situative/adaptive strategies for online application. Rule optimization can be conducted qualitatively to define most relevant set of control variables, or quantitatively to yield optimal values for each variable [6]. However, this approach is sensitive to driving conditions with different dynamics and requires large database to improve its performance [7].

On the other side, adaptive rule-based (ARB) methods are capable of handling a broad spectrum of driving conditions and achieve near optimal results [13]. The working principle of ARB methods can be pointed out as follows: First, driving states are defined based on a set of characteristic features

Manuscript received XXX, XX, 2021; revised XXX, XX, 2021. *(corresponding author: Ahmed M. Ali.)*

Ahmed M. Ali is with the Automotive Engineering Department, Military Technical College, Cairo, Egypt. (E-mail: ahmed.m.ali@mtc.edu.eg)

Bedatri Moulik is with the Department of Electrical and Electronics Engineering, Amity university, Sector 125, 201303 Noida, India.

Dirk Söffker is the head of Chair of Dynamics and Control, University of Duisburg-Essen, Duisburg, 47057, Germany

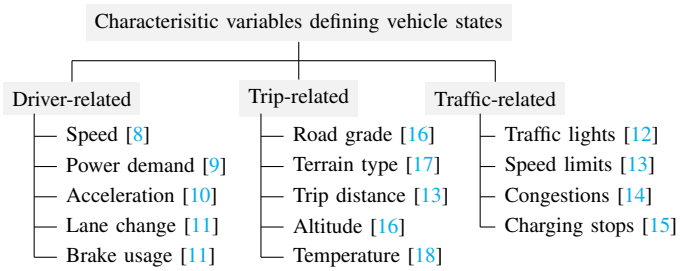

Fig. 1: Characteristic variables defining vehicle states for adaptive rule-based PMS [13]

(variables) from standard driving cycles; second, optimal power management strategies for respective vehicle states are determined using offline optimization; third, optimized solutions are implemented as look-up tables within the online control scheme; fourth, driving situations in real-time application are recognized and matched to vehicle states and hence, respective control strategies can be applied [19].

One of the advantages of decoupling optimization as an offline process and power management as an online process is the ability to implement global optimal solutions into real-time control schemes. Typically, evolutionary algorithms are suitable for multi-objective optimization of PMS goals, i.e. electric energy efficiency, driving performance, and battery life. Computational efficiency plays a vital role for the real-time applicability of ARB algorithms. In this context, minimization of time and memory usage is essential. This aspect has been investigated in [20] for three online PMSs, revealing that implemented adaptive co-states for equivalent consumption minimization strategy (A-ECMS) has a significant impact on the performance of such ADR methods. The precomputation of parameters in an offline process also reduces the computational effort.

In [21], control variables are optimized offline as a decoupled process and used to tune the controller for online use, achieving optimal distribution between three HEV powertrain sources such that dynamic parts of the load are supplied by the supercapacitor. The decoupling of the optimization process from the online process enables the use of offline-implementable, multi-objective algorithms. Due to the modular structure of power management optimization concept, an extension of the concept to unknown vehicle states can be realized by integrating look-up tables (LUTs) with sets of optimized parameters. Dynamic behavior of energy sources in EV is a crucial aspect of PMS, which has been addressed in [22], tacking into account past driving patterns. In [23], it has been investigated that online, real-time-based strategies only provide suboptimal solutions, and hence a global optimization-based, real-time-based strategy was developed with lower computational effort compared to dynamic programming. Low computational effort was guaranteed by computing a part of the algorithm offline. However, the assumption is that the drive cycle has to be known in advance.

Selection of characteristic variables defining vehicle states is a critical aspect of ARB methods. Besides, optimal discretization levels for each variable has a non-negligible impact on

TABLE I: Implemented characteristic variables for ARB algorithms [25]

	Characteristic variables											
Ref.	Speed			Power demand			Driver style			Trip		
	Average	Range	St. deviation	Average	Range	St. deviation	Idle time	Cruise time	Acc. time	Gradient	Distance	Duration
[26]	●	●	●	●	●	●				●		
[27]	●	●	●	●	●	●	●	●	●			●
[28]	●			●				●				●
[29]	●	●		●							●	●
[30]	●	●		●		●	●	●	●			
[25]	●		●	●		●			●			
[31]	●	●	●	●	●	●	●	●	●		●	
[32]	●	●	●		●	●		●	●		●	●

the accuracy of state recognition and the suitability of defined control strategies [13]. The review of relative contributions in literature give an insight into a set of characteristic variables used to define vehicle states for ARB strategies as illustrated in Fig. 1.

Characteristic variables for vehicle state definition fall into three main categories: driver-based, trip-dependent, and traffic-related variables [24]. It has been evinced, that fuel economy in EVs is considerably affected by driver-based variables, i.e. maneuvering style, coasting, acceleration, and brake usage [8]–[11]. Statistical measures for repetitive lane changing, brake pedal abuse, and driving speed are used to identify driver's style and hence, suitable power handling solution can be defines accordingly [13].

Traffic-related information has been gaining increasing attention in light of recent advances in vehicular communication technologies, intelligent transportation systems (ITS), and the rapidly-growing Internet-of-Vehicles (IoV) [33]. Optimal driving speed and power demand can be defined a priori for upcoming route-sections based on the foreknowledge about traffic congestions and speed limits [34]. Likewise, information about road grade, trip distance, and available charge locations can be implemented to define optimal usage of on-board energy [16]–[18].

Online recognition of vehicle states has been conducted in literature using different pattern recognition algorithms. To this aim, fuzzy logic has been widely implemented due to its accuracy and attainable computational requirements [35]. Support vector machines (SVM) and Artificial neural networks (ANN) are rather used to handle large amounts of data-inputs and to ensure optimal clustering of driving patterns [33]. A reinforcement learning (RL)-based strategy has been implemented along with Markov chains in [36], achieving a reduction in energy loss compared to rule-based strategy. Finite-state machine has been implemented to ARB to improve the ability to adapt to varying driving patterns by determining the switching between event-triggered rules [13]. In [37], a NN-based drive pattern prediction is combined with optimized

power management to minimize both energy loss and battery degradation in an EV.

The review of literature puts forward the significance of particular characteristic variables defining driving patterns in ARB methods as illustrated in Table I. Statistical attributes of speed and power demand have been widely implemented to define discrete driving patterns and speed profiles. Besides, duration of cruising, idling, and speed-ups have been particularly implemented to gain useful insights about driver style [26]–[32]. Trip duration and distance have been more relevant to ARB methods than other characteristics in literature to define suitable power handling rules for specific trips [25].

The impact of characteristic variables on solution optimality in ARB methods has been thoroughly investigated in literature, putting forward the potential to improve energy efficiency in EVs using certain combinations/discretization levels of such variables [19]. Besides, defining vehicle states in terms of multiple characteristic variables is beneficial for the accuracy of pattern recognition and the adequateness of adapted power management rules [13].

B. Problem statement and main contribution

The presented review of literature reveals the significant potential of adaptive rule based PMS to improve driving performance and energy efficiency of electrified powertrains. Despite the increasing focus on situative PMS,two main challenges are still not addressed in literature: First, defining optimal set of characteristic variables for ARB with suitable discretization levels; and second, evaluation and assessment of optimally-situated PMS for different driving cycles.

This contribution aims at tackling the above-mentioned challenges as follows: first, an intelligent PMS is proposed, whereby optimal set of characteristic variables defining vehicle states has been considered. Second, discretization levels for each variable is investigated to give useful insights into the representation of different states during vehicle operation. Offline optimization of power management rules is conducted for each vehicle state. Third, evaluation and assessment of proposed PMS is conducted using different types of driving cycles to put forward the achieved improvement under different operating conditions.

The organization of this paper can be summarized as follows: description of implemented model for electric FCV and respective emulation test-bench is given in Section II. The proposed PMS is explained in Section III, followed by the analysis of results and discussion in Section IV.

II. MODELING, CONTROL, AND EMULATION OF FUEL CELL ELECTRIC DRIVELINE

A multi-source pure electric powertrain model is considered for this work, comprising fuel cell, battery, supercapacitor, traction motor, and DC/DC converters. Validation of the dynamic behavior of driveline components under different control strategies has been conducted using a hardware-in-the-loop (HiL) experimental test-rig in [38]. Characteristics of different driveline components have been summarized in Table II.

Emulation of driveline components, i.e., battery, fuel cell, supercapacitor, and a 4Q-motor-generator has been realized using controllable power sources and sinks. The degree of similarity between the simulated and emulated values of investigated variables has been used to validate different control schemes for FVCs [38]. More details about driveline modeling and description of the emulation test-rig is given in the sequel.

A. Modeling of a full-active fuel cell electric powertrain

The implemented FCV model in Fig. 2 comprises a full–active driveline with three independent DC/DC converters connected to the fuel cell, the battery, and to the supercapacitor [38]. The role of PMS is to provide the desired values of fuel cell, battery, and supercapacitor currents, based calculated power demand.

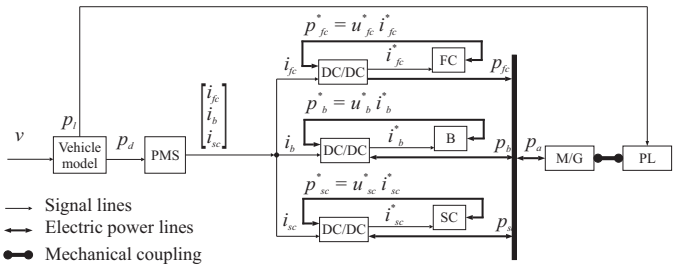

Fig. 2: Drive-line configuration and power flow scheme of the fuel cell hybrid vehicle [30].

The power demand P_d is calculated as a product of driving cycle speed v and tractive force f_T as,

$$P_d = f_t\ v \tag{1}$$

where, f_t is given by,

$$f_t = m\dot{v} + mg\phi\cos\alpha + \frac{\rho\ A_f c_d v^2}{2} + mg\sin\alpha, \tag{2}$$

where m denotes vehicle mass, g the gravitational acceleration, α road inclination, ρ air density, A_f vehicle frontal area, and c_d is drag coefficient of the vehicle. The actual delivered power P_a is calculated based on the ratio of power synergy from the fuel cell P_{fc}, the battery, P_b, and the supercap. P_{sc} as,

$$P_d = P_{fc} + P_b + P_{sc}, \tag{3}$$

whereby the fuel cell power is calculated considering the power losses through activation, ohmic, and concentration voltages as [38],

$$u^*_{fc} = n_c(u^o_{fc} - \underbrace{\left(c_1 + c_2\left(1 - e^{-i^*_{fc}c_3}\right)\right)}_{u_{act}} - \ldots$$
$$\underbrace{i^*_{fc}\ R_{fc}}_{u_{ohm}} - \underbrace{i_{fc}\left(\frac{c_4\ i^*_{fc}}{i_{max}}\right)^{c_5}}_{u_{conc}}), \tag{4}$$

where, n_c denotes the number of stack cells, u^o_{fc} the no-load voltage, i_fc fuel cell current, R_{fc} ohmic resistance of the fuel cell, $c_3 = 10$, $c_5 = 2$, c_1, c_3, c_4 are defined according to quasi-static levels of fuel cell temperature using look-up tables [39, 40], and the notation * signifies in general the inputs to

each DC/DC converter. Battery modeling has been conducted based on a second-order Thevenin model as illustrated in Fig. 3.

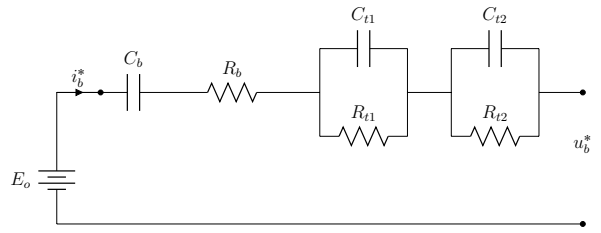

Fig. 3: Equivalent circuit model of the battery based on second-order Thevenin model [41]

Second-order Thevenin model (also referred to in literature as PNGV model [42]) has been widely implemented for modeling of electric batteries in vehicular traction systems due to its ability to represent the ohmic behavior and electrochemical polarization with high fidelity and low computational requirements [43, 44]. Terminal voltage of the battery u_b^* (before the DC/DC converter) can be described as

$$u_b^* = E_o - i_b^*\ R_b - u_{t1} - u_{t2} - \frac{1}{C_b}\int_{t_i}^{t_f} i_b^*\ dt, \tag{5}$$

whereby the open-circuit battery voltage is considered at no-load as $u_b^o = E_0$, R_b denotes the internal resistance of the battery, C_b the fictive capacitance representing the changes in electromotive force, $u_b^*(t)$ the terminal voltage, and the battery polarization is modeled through two consecutive RC-networks, such that the voltage dynamics across each RC circuit can be defined as

$$\begin{bmatrix}\dot{u}_{t1}\\ \dot{u}_{t2}\end{bmatrix} = \begin{bmatrix}-\frac{1}{R_{t1}C_{t1}} & 0\\ 0 & -\frac{1}{R_{t2}C_{t2}}\end{bmatrix}\begin{bmatrix}u_{t1}\\ u_{t2}\end{bmatrix} + \begin{bmatrix}\frac{1}{C_{t1}}\\ \frac{1}{C_{t2}}\end{bmatrix} i_b^*, \tag{6}$$

where $R_{t1,t2}$ and $C_{t1,t2}$ denote the equivalent resistance and capacitance of each polarization RC-network [45].

For the supercapcitor, a dynamic model (adopted from a 3-stage ladder model) is considered comprising two RC-networks ($R_{s1,s2}$ and $C_{s1,s2}$), a bulk capacitance C_{sc} , and an ohmic resistance R_{sc} as shown in Fig. 4 [46, 47].

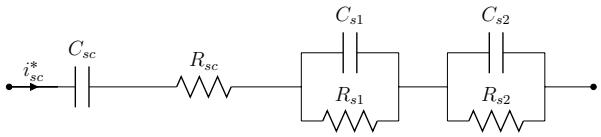

Fig. 4: Equivalent circuit model of the supercapacitor based on an advanced 3-stages ladder mode (Dynamic Randle model) [46, 47]

The impedance across the RC-networks represent the double-layer capacitance and charge transfer at high dynamic rates [48]. It is noticeable that the number of in-series RC-networks in such models can be increased to improve model accuracy at high-frequency operations [49, 50]. The dynamic model is capable of capturing the transient charging/discharging dynamics of supercapacitors over a wide range of operating frequencies, and hence have been widely implemented for simulation and analysis of electric driveline models. Output voltage of the supercap. is given by

$$u_{sc}^* = u_{sc}^o - i_{sc}^*\ R_{sc} - u_{s1} - u_{s2} - \frac{1}{C_{sc}}\int_{t_i}^{t_f} i_{sc}^*\ dt, \tag{7}$$

where i_{sc}^* denote withdrawn current from the supercapacitor. The voltage dynamics of each RC-network can be formulated as

$$\begin{bmatrix}\dot{u}_{s1}\\ \dot{u}_{s2}\end{bmatrix} = \begin{bmatrix}-\frac{1}{R_{s1}C_{s1}} & 0\\ 0 & -\frac{1}{R_{s2}C_{s2}}\end{bmatrix}\begin{bmatrix}u_{s1}\\ u_{s2}\end{bmatrix} + \begin{bmatrix}\frac{1}{C_{s1}}\\ \frac{1}{C_{s2}}\end{bmatrix} i_{sc}^*. \tag{8}$$

Modeling parameters of battery and supercapacitor models in Eqns. (5)–(8) have been identified and experimentally validated using real driveline components of the emulation test-rig with the values shown in Table II [40].

In light of given battery and supercapacitor models, the state of charge of both components can be calculated as

$$\begin{bmatrix}SoC_b\\ SoC_{sc}\end{bmatrix} = \begin{bmatrix}SoC_{b0}\\ SoC_{sc0}\end{bmatrix} - \begin{bmatrix}\frac{1}{Q_{b0}} & 0\\ 0 & \frac{1}{Q_{sc0}}\end{bmatrix}\begin{bmatrix}\int_{t_i}^{t_f} i_b^*\ dt\\ \int_{t_i}^{t_f} i_{sc}^*\ dt,\end{bmatrix} \tag{9}$$

where the initial charge of the battery and supercapacitor are denoted by SoC_{b0} and SoC_{sc0} and the nominal charge in each source is Q_{b0} and Q_{sc0} respectively.

The input/output relation of implemented DC/DC converters is described as

$$i_{in} = i_{out}\ \frac{u_{bus}}{u_{in}}\ \frac{1}{\mu_{conv}}, \tag{10}$$

where desired bus voltage is given as c_6 and the quasi-static conversion efficiency is defined as a look-up table $\mu_{conv} = f(i_{in}, i_{out}, u_{in}, u_{out})$. Constant bus voltage has been retained using a PI-controller of the DC/DC converters such that

$$P_d = I_d \cdot u_{bus}, \tag{11}$$

whereby, the PMS defines required current delivery from each source as

$$I_d = \begin{bmatrix}i_{fc}^* & i_b^* & i_{sc}^*.\end{bmatrix}^T \tag{12}$$

A simplified mathematical model for the brushless DC motor is given by a single input/multiple output (SIMO) state space form as,

$$\dot{x} = A_m x + B_m u, \tag{13}$$
$$y = C_m x + D_m u, \tag{14}$$

for

$$x = \begin{bmatrix}\omega & i_m\end{bmatrix}^T,\ u = u_m(t), \tag{15}$$

$$A_m = \begin{bmatrix}-\frac{b_m}{J} & \frac{k_{eq}}{J}\\ -\frac{k_{eq}}{L} & -\frac{R_m}{L}\end{bmatrix},\ B_m = \begin{bmatrix}0\\ \frac{1}{L}\end{bmatrix}, \tag{16}$$

$$C_m = \begin{bmatrix}1 & 0\\ 0 & 1\end{bmatrix},\ \text{and}\ D_m = \begin{bmatrix}0\end{bmatrix}, \tag{17}$$

where b_m denotes the viscous friction constant, k_{eq} the electromotive force constant, L equivalent circuit inductance, J the rotational moment of inertia, and R_m is the equivalent circuit resistance. Numerical value of all modelling parameters are provided in Table II.

TABLE II: Characteristic of driveline components

Component	Specs/Modeling parameter		Value	
Vehicle	Curb mass	(m)	1500	[kg]
	Frontal area	(A_f)	2	[m^2]
	Coeff. of rolling res.	(ϕ)	0.007	[–]
	Air density	(ρ)	1.27	[kg/m^3]
	Drag coefficient	(c_d)	0.3	[–]
	Tire radius		0.323	[m]
Fuel cell	Type		PEM	
	Rated power		1.2	[kW]
	Output voltage range		22–50	[V]
	Rated power		1.2	[kW]
	Number of modules	n_c	45	[–]
	Max. output current/cell		2.2	[A]
	Ohmic resistance	R_{fc}	0.08	[Ω]
Battery	Type		Li-ion	
	No. of modules		33	
	Max. cell voltage		4.2	V
	Ohmic resistance	R_b	0.09	[Ω]
	Fictive capacitor	C_b	43.2	[kF]
	1^{st} polarization resistance	R_{t1}	0.060	[Ω]
	1^{st} polarization capacitor	C_{t1}	366.3	[F]
	2^{nd} polarization resistance	R_{t2}	0.058	[Ω]
	2^{nd} polarization capacitor	C_{t2}	2.98	[F]
	Initial SoC	SoC_{b0}	60	[%]
Supercap.	Nominal voltage		14	V
	No of modules		72	
	Nominal capacity		350	[F]
	Ohmic resistance	R_{sc}	0.008	[Ω]
	Bulk capacitance	C_{sc}	3	[kF]
	1^{st} polarization resistance	R_{s1}	0.002	[Ω]
	1^{st} polarization capacitor	C_{s1}	23	[F]
	2^{nd} polarization resistance	R_{s2}	0.004	[Ω]
	2^{nd} polarization capacitor	C_{s2}	300	[F]
	Initial SoC	SoC_{sc0}	66.7	[%]
Motor	Type		BLDC	
	Rated voltage		400	[V]
	Rated angular speed		3500	[RPM]
	Viscous friction constant	b_m	0.0012	[N.m.s]
	Electromotive force constant	k_{eq}	0.065	[V/rad/sec]
	Equivalent circuit inductance	L	0.5	[mH]
	Rotational moment of inertia.	J	0.0122	[kgm^2]
	Equivalent circuit resistance	R_m	0.9893	[Ω]

B. Emulation principle and experimental implementation

The electric FCV driveline has been experimentally emulated using the HiL test-rig shown in Fig 5. The emulation test-rig interfaces the described driveline model (in MATLAB/Simulink) with respective hardware components, i.e. battery, supercapacitor, fuel cell, drive motor, and programmable load through CAN-Bus communication using dSPACE DSPs . The emulation test-rig illustrated in Fig. 5 has been developed at the Chair of Dynamics and Control (SRS), University of Duisburg-Essen [38].

The dynamic behavior of FCV drive-line is emulated using a power source–sink set for each power source to perform the power flow processes, i.e. charging, discharging, and power consumption. Besides, developed power management strategies are depicted into the emulation test-rig for online application of different PMS and to verify the impact of different power handling decisions on the dynamic behavior of driveline components. However, the real-time applicability of different control algorithms can not be ensured in this sense using the emulation test-rig, due to the difference in computational capabilities between industrial vehicular computers and the implemented DSP of the test-rig. Therefore, assessment of the computational requirements for developed power management algorithms should be explicitly performed [30].

III. INTELLIGENT ADAPTIVE POWER MANAGEMENT

A. Background and novel improvements

The proposed concept is designed to provide near-optimal power management strategy for most of the driving patterns encountered during urban, suburban, and highway conditions. To this aim, working steps of proposed adaptive PMS can be defined as follows: Characteristic variables for different trip conditions, i.e. number of stops, average and standard deviation of speed and acceleration $\bar{v}$, $\sigma(v)$, and $\sigma(a)$ accordingly, total distance d_{tot}, and trip duration t_{DC} are extracted using a set of 25 driving cycles as illustrated in Table III.

TABLE III: Characteristic of driving cycles for grid-space structure [13]

	t_{DC} [s]	d_{tot} [km]	v_{max} [km/h]	$\sigma(v)$ [km/h]	No. of stops	a_{max} [ms^{-2}]	$\sigma(a)$ [ms^{-2}]
Min.	85	0.13	14	1	1	0.2	0.16
Max.	1766	46.2	138	38	23	0.7	0.55

Extracted features are depicted as axes into a multi-dimensional space, referred to as grid-space (GS), whereby each point in GS refers to a vehicle state. In this context, the interpretation of drive state recognition in terms of suitably defined variables is a viable solution for the contradicting accuracy/applicability problem. Based on the defined states in GS, representative segments are generated to reflect corresponding driving conditions. These segments are implemented for offline optimization of power management rules, according to defined cost function(s).

The structure of GS, in terms of depicted axes and respective discretization levels, is a crucial aspect that influences the ability to yield optimal power management solutions. Thus, optimal structure of GS has been investigated in a previous step of this work considering five characteristic variables at different discretization levels [13]. The analysis of variance (ANOVA) for more than 150 constellations of grid-space axes in [13] put forward a significant impact of specific characteristic variables to be implemented for adaptive RB-PMS, namely: vehicle speed, power demand, and speed dynamics. Representation of recognized vehicle states in grid-space is exemplified in Fig. 6, considering arbitrary levels of axes' discretization.

In this contribution, the main findings of [13] regarding grid-space structure has been considered as a base for the proposed adaptive RB-PMS, whereby two further improvements has been conducted: first, definition of vehicle states in grid-space has been evaluated using cluster analysis of recognized states; second, application of proposed PMS to different types of driving cycles to give further insights into the suitability of optimized power management rules for unknown driving conditions as summarized in Fig. 7.

For such data-intense PMS, k-mean clustering of driving conditions in grid-space plays a crucial role for defining optimum power management strategies for similar vehicle states [25]. To this aim, clustering of recognized states in grid-

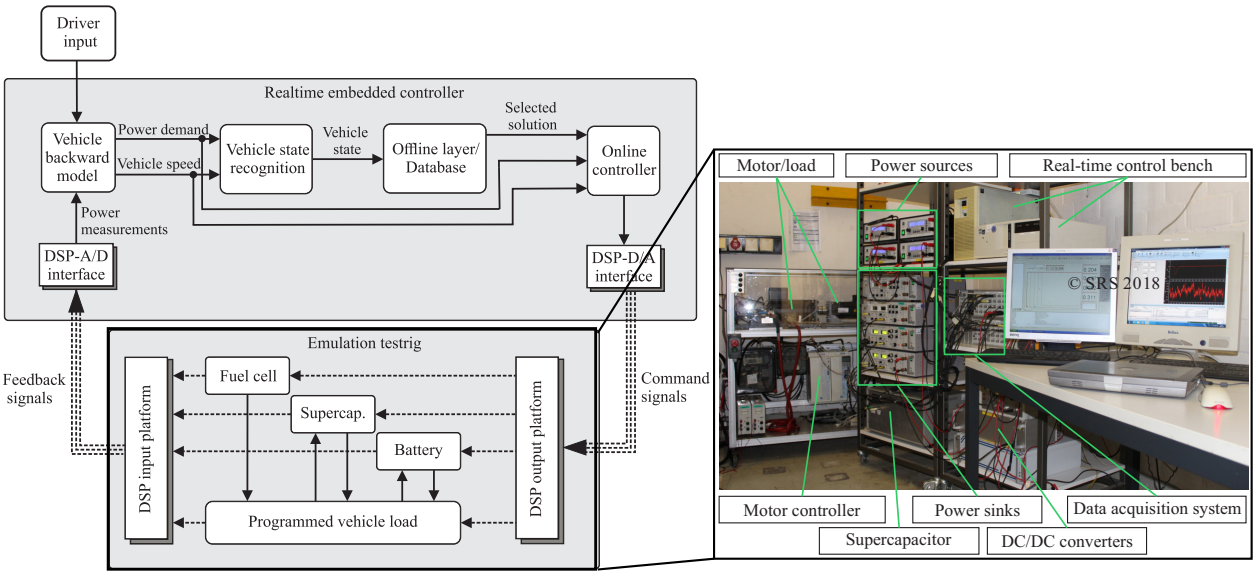

Fig. 5: Operation scheme of the multi-source hybrid powertrain in hardware-in-the-loop test-bench

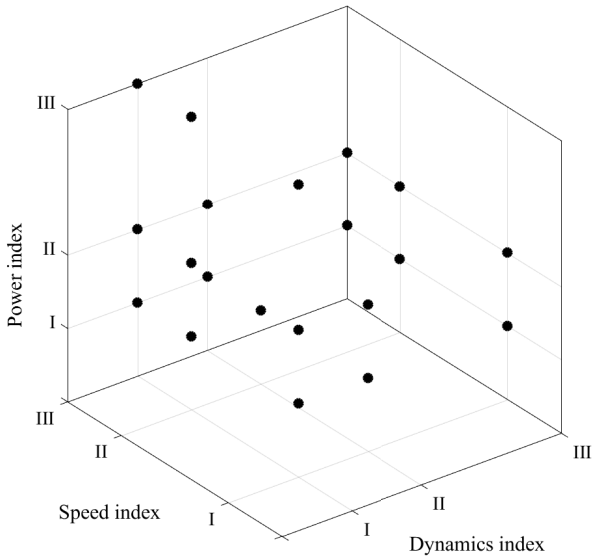

Fig. 6: Recognized vehicle states in grid-space during US06 drive cycle

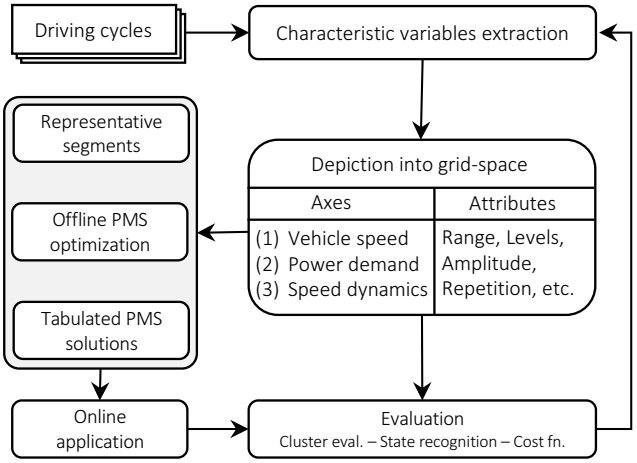

Fig. 7: Generation of grid-space using a set of driving cycles and iterative evaluation.

space has been conducted considering a range of candidate clusters $\{G_1, G_2, ..., G_n\} \subset \mathbb{R}^3$, whereby

$$G_i \nsubseteq \varnothing \tag{18}$$

$$G_i \cap C_j = \varnothing \text{and} \tag{19}$$

$$\bigcup_{i=1}^{n} G_i = \chi, \tag{20}$$

for $i, j = 1, 2, ..., n$ and $i \neq j$, where χ denotes the set of recognized vehicle states in grid-space. K-means++ algorithm has been implemented to calculate clusters' centroids iteratively based on the Euclidean distance in grid-space [51]. Defining an optimal number of clusters n^* is a well-known challenge in literature due to the contradictive relation between clustering accuracy (for large n) and data compression within each cluster (for small n) [52]. Therefore, cluster evaluation based on Calinski-Harabasz index has been considered to provide a quantitative measure of the ratio between the inter-group variance and the intra-group variance of state-clusters. The results og k-means clustering based on Calinski-Harabasz index is illustrated in Fig. 8, revealing an optimal number of $n^* = 9$ for state-clusters in grid-space.

B. Offline optimization of power management rules

Based on defined vehicle states in grid-space, representative segments can be artificially synthesized corresponding to respective characteristic variables. To define optimal operating conditions for specific drive state, the optimization task can be formulated as a multi-variable/multi-objective problem to

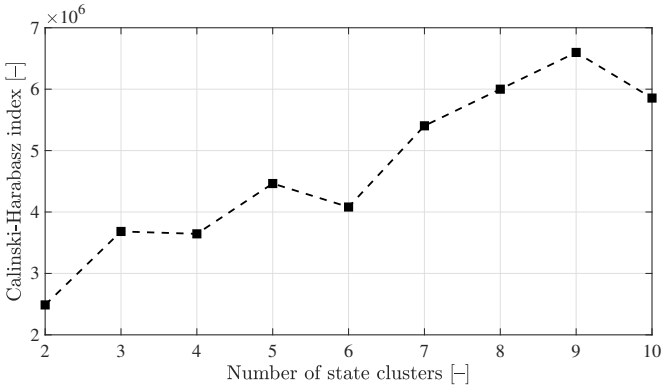

Fig. 8: Defining optimal number of vehicle state clusters based on Caliniski-Harbasz index.

yield minimal fuel consumption and final drop of the battery's state of charge as follows

$$\begin{aligned} &\min \quad J, \\ &\text{where} \end{aligned}$$

$$J = \begin{bmatrix} \underbrace{\alpha \int_{t_i}^{t_f} \dot{m}_{eq}(x_{1-4}, t)dt}_{obj_1} \\ \underbrace{\beta\, \Delta SoC(x_{1-4,0}, x_{1-4,f}, t_i, t_f)dt}_{obj_2} \end{bmatrix}, \tag{21}$$

subject to

$$x_1(t) \quad \in [I_{fc,min}, I_{fc,max}], \tag{22}$$
$$x_2(t) \quad \in [\zeta_{min}, \zeta_{max}], \tag{23}$$
$$x_3(t) \quad \in [I^L_{b,min}, I^U_{b,min}], \tag{24}$$
$$x_4(t) \quad \in [I^L_{b,max}, I^U_{b,max}], \tag{25}$$
$$x_{1-4}(0) = x_{1o-4o}, \quad \text{and} \tag{26}$$
$$x_{1-4}(t) \subset \Re^n, \tag{27}$$

where SoC denotes the battery state of charge, m_{eq} the equivalent fuel consumption, α and β weighting factors, and t_i and t_f are the initial and final time respectively, and the suffices L and U denote lower and upper limits of corresponding variable.

Both objectives of the cost function J have been defined to ensure minimal energy consumption without scarifying driveability requirements and not get trapped into charge-depletion/charge sustaining strategy. The first objective obj_1 reflects total hydrogen mass consumption of the fuel cell, that is the prime mover of the vehicle and the recharging source of the battery and supercapacitor. Defining the second objective obj_2 in terms of the charge drop ΔSoC has been considered to tackle the divergence into the trivial solution, that is constantly depleting the battery and supercharge to minimize hydrogen consumption, until lower limits of SoC is reached, then operating the fuel cell inefficiently to deliver traction energy and recharge ESS.

The problem is solved using non-dominant sorting genetic algorithms (NSGA-II) on a Cruncher-Workstation considering 50 discrete levels for each variable $x_1 - x_4$ over 100 generations. Results from offline optimization of Eqns. (21)–(22) are exemplified in Fig. 9 for a single vehicle state, revealing the aforementioned contradiction between minimizing depleted energy from the fuel cell and retaining the charge of the battery and supercapacitor at the end of each driving cycle. In this sense, the optimal solution can be simply defined as the minimal Euclidean distance from the origin of Pareto front (considering equal weights for obj_1 and obj_1).

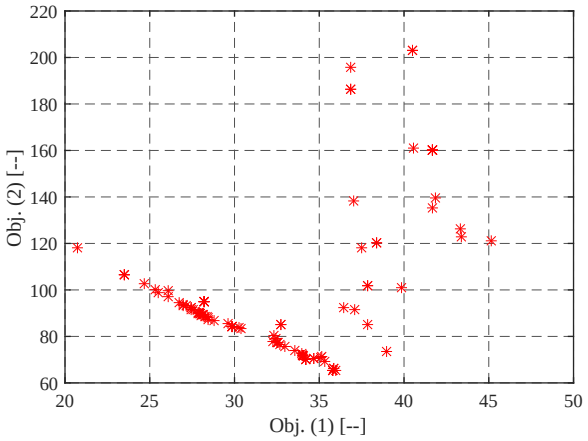

Fig. 9: Optimization results for an exemplified vehicle state using NSGA-II in offline layer

To decouple the complexity of solving Eqns. (21)–(22) online, the optimization problem is solved offline for all vehicle states in grid-space and the final solutions are mapped to according driving conditions to be addressed by the real-time controller. Optimal power management solutions are integrated into the online controller in form of multiple LUTs.

C. Online application and supervisory control

Optimally-defined power management rules are integrated into the online control as look-up tables (LUTs), whereby recognized driving conditions from real trips can be handled according to corresponding control strategies from optimized LUTs. The benefit of this concept lies at the mitigated computational effort required. The easy switching between the tabulated solutions by using a suitable algorithm makes it possible to realize this online and in real-time.

During online power management, the recognition process in real-time layer considers two main aspects: recent and a finite horizon of previous characteristic variables' clusters. Once a specified drive state is detected, the corresponding solution is restored to update the rule-based optimization constrains. During transient conditions, the cluster length is re-initiated to avoid divergence of solution optimality. Also, the current unknown drive cycle can be stored and optimized in the offline layer for enhancement of grid-space structure.

The introduced control scheme has been implemented as a Matlab/Simulink model as shown in Fig. 10. Operating conditions, i.e. power demand, vehicle speed, and state of charge are used to define respective vehicle state in grid-space and hence, optimal power management strategy can

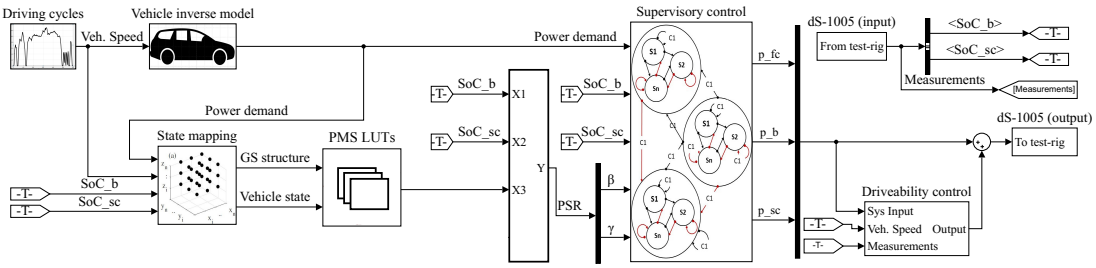

Fig. 10: Adaptive rule-based (Ad-RB) power management system of a fuel cell hybrid powertrain implement in Matlab/Simulink model.

be extracted. A supervisory control module is implemented to ensure suitable operating boundaries for driveline components, as explained in the sequel. Driveability control is performed before the DSP-interface with the emulation test-rig, to ensure fulfillment of power demand and optimal profile tracking of the driving cycle speed.

The conformity of optimized solutions is checked through the supervisory control module w.r.t. operating limits of each power source and driveline component [53]. To this aim, power demand is used to interpret the status of driving mode, i.e., acceleration ($P_d > 0$), braking ($P_d < 0$), or stopped ($P_d = 0$). Besides, the value of SoC_b and SoC_{sc} implies the readiness of the battery and the supercapacitor to deliver or receive energy during traction or regenerative braking. Optimized power management strategies for vehicle states comprise a customized solution for each mode of operation as shown in Table IV. Accordingly, different modes of operation for each energy source can be defined

TABLE IV: Modes and corresponding actions

Mode	Action	Components	Task
1	Acceleration	Battery + Supercap.	Charge
2		Battery	No discharge
3		Supercap.	No discharge
4		Battery + Supercap.	Discharge
5		Battery + Supercap.	Standard
6	Braking	Supercap.	Charge
7		Battery	Charge
8	Stop	Supercap.	Charge
9		Battery	Charge

The supervisory control is deployed as a state machine program, whereby transition between states is defined based on P_d according to respective mode in Table IV. In this sense, both vehicle states and modes are defined during online operation to yield optimal power management decisions and to ensure applicability of such decisions as exemplified for driving cycle (us06) in Fig. 11.

IV. RESULTS ANALYSIS AND COMPARATIVE EVALUATION

In order to investigate the proposed control strategy under different trip conditions, three driving cycles have been selected,

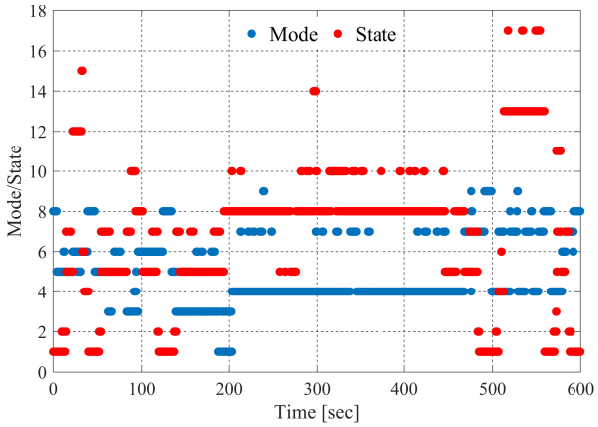

Fig. 11: Controller modes / recognized states during US06

TABLE V: Characteristics of considered driving cycles for the comparative evaluation

	Driving cycles		
	Modem IM-short	HWFET	NEDC
Type	Urban	Highway	Mixed
d_{tot} **[km]**	2.20	16.5	11.0
t **[s]**	255	765	1180
$\overline{v}$ **[km/h]**	31.8	77.7	33.6
v_{max} **[km/h]**	68.9	96.3	120
$\overline{a^+}$ **[m/s^2]**	0.53	0.16	0.53
$\overline{a^-}$ **[m/s^2]**	0.59	0.18	0.72
# $a^+ = 0$	8	26	31
# Stops	5	1	14
$\overline{t_s}$ **[s]**	5.60	1.00	17.2

representing urban (modemIM short), highway (HWFET) and mixed driving conditions (NEDC). Characteristics of selected driving cycles are summarized in in Table V including total traveled distance d_{total}, trip duration t, average speed $\overline{v}$, maximum speed v_{max}, number of accelerations $\#a^+ = 0$, average stop duration $\overline{t_s}$, and average positive– and negative acceleration $\overline{a^+}$ and $\overline{a^-}$ accordingly. Moreover, the analysis of results in this section is more concerned with physical values, i.e. energy consumption and state of charge for the battery and supercapacitor, rather than the mathematical terms of the cost function in Eqns. (21)–(22), to avoid misinterpretation of

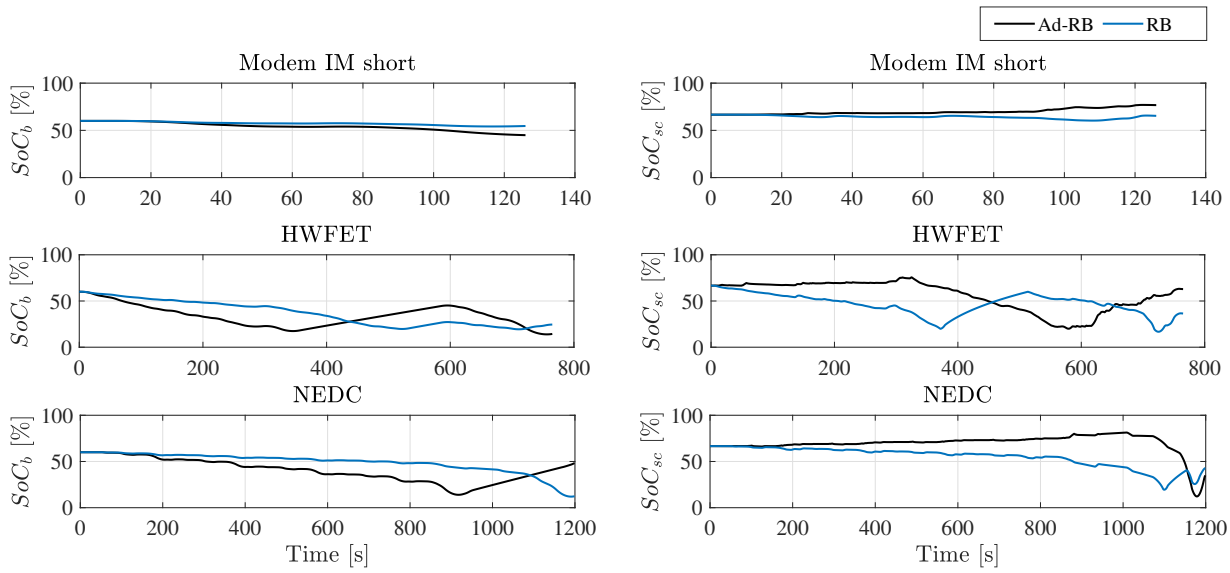

Fig. 12: State of charge profiles of the battery and supercapacitor under ARB and RB PMS for different driving cycles.

normalized terms in the latter.

The state of charge profiles for the battery and supercapacitor are illustrated in Fig. 12 for conventional rule-based (RB) and proposed adaptive rule-based (Ad-RB) PMS. Calculation of SoC_b and SoC_{sc} has been conducted according to Eqn. (5)–(9), which has been comparatively verified to respective measurements from the emulation test-rig [13]. The figure shows higher tendency of Ad-RB to provide synergy power from the battery and implement supercapacitor's power to take over unscheduled power demands (particularly for highway driving cycles). This strategy more perceivable in highway and mixed driving cycles with longer trip durations and higher power demand; whereby, the role of supercapacitor is more relevant.

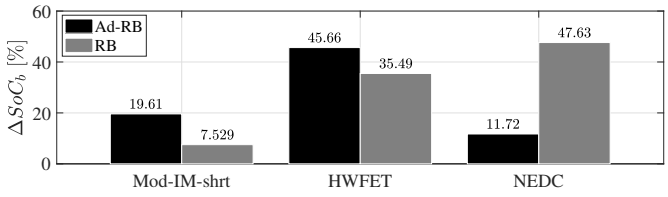

Fig. 13: Final drop in SoC_b under ARB and RB PMS for different driving cycles.

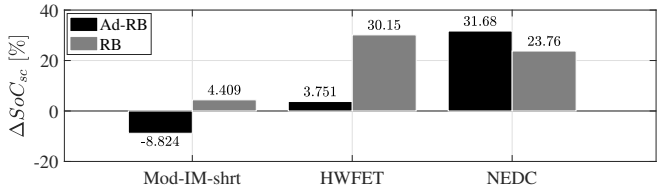

Fig. 14: Final drop in SoC_{sc}under ARB and RB PMS for different driving cycles.

The drop in SoC_b and SoC_{sc} is comparatively evaluated for both ARB and RB strategies in Fig. 13. and Fig. 14. It can be perceived from Fig. 13 that higher depletion of SoC_b has been reached using ARB strategy for nearly all driving cycles. Accordingly, the supercapacitor has been implemented to recuperate more energy at the end of each driving cycles, compared to the conventional rule-based strategy. For short urban trips, a drop of $\Delta SoC_b = 19.6\%$ has been reached with an opportunity to recuperate more energy into the supercapacitor, leading to an increase of $+8.8\%$ in SoC_{sc}. For highway driving cycles, a drop of 45% ΔSoC_b has been reached, which reflects the increasing need for synergy power from auxiliary sources. It is noticeable that, in order to avoid the concurrent depletion of both energy sources, the drop in SoC_b and SoC_{sc} has been represented as a normalized sum of both values in the conducted offline optimization (see Obj_2 in Eqn. (21)).

The synergy ratio for the battery and supercapacitor under different control strategies ($\frac{\text{Provided energy by each auxiliary source}}{\text{Total consumed energy for the driving cycle}}$) is illustrated in Fig. 15. The achieved results puts forward the main difference between conventional power splitting (based on heuristic ratios) and offline-optimized strategies as the increase in synergy tasks of the battery and retaining sufficient energy in the supercapacitor, that acts as a buffering reserve to avoid excessive overloading of the fuel cell. This can be perceived through the decreased synergy ratio of the SC for all driving cycles (except for NEDC), which reflects the increase of SoC_{sc} at the end of each driving cycle.

Energy consumption in electrified vehicles is a relevant and objective measure for comparative evaluation of different power management strategies. Therefore, energy consumption over testing driving cycles for both Ad-RB and RB PMSs are illustrated in Table VI. Moreover, the global optimal solution using NSGA-II for each driving cycle (based on the cost function in Eqn. (21)) has been provided, to give more insights into the achieved level of optimality using Ad-RB algorithm.

The comparison gives a clear insight into the impact of driving cycle type on achievable performance of proposed

ARB algorithm. For urban and highway trips, the improvement in energy consumption is 13.6 – 14.6 %. On the other side, an improvement of 30.89 % in energy consumption has been achieved for mixed driving cycles. This reduction in energy consumption reflects a near-optimal performance (> 99 % match) of Ad-RB PMS at different types of trip conditions. The illustrated performance of Ad-RB methods puts forth the potential of state-oriented PMS using grid-space representation to provide near-optimal power management solutions during online operation of electric vehicle.

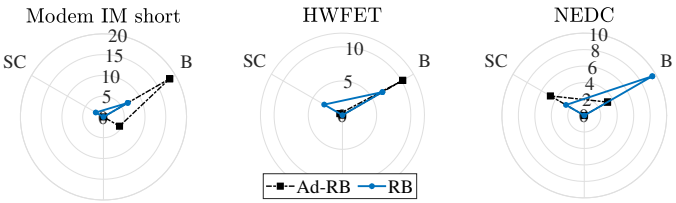

Fig. 15: Synergy ratio in [%] of battery's (B) and supercapacitor's (SC) energy for different driving cycles.

TABLE VI: Energy consumption for selected driving cycles under different control strategies.

	Driving cycles		
	Modem IM-short	HWFET	NEDC
Type	Urban	Highway	Mixed
E^* **[kWh/100km]**	30.33	20.33	23.41
E_{rb} **[kWh/100km]**	40.50	25.50	36.34
E_{ad-rb} **[kWh/100km]**	34.99	21.77	28.02
Improvement† **[%]**	13.60	14.61	30.89
Optimality ‡ **[%]**	99.54	99.72	99.73

† Compared to rule-based solution

‡ Compared to global optimal solution (NSGA-II)

V. Conclusion

In this contribution, an intelligent power management strategy has been proposed to approach optimal power handling decisions in real-time applications. The proposed method is based on defining a set of representative vehicle states in a multi-dimensional space (grid-space), to which optimal control variables are optimized offline. For online application, vehicle states can be recognized based on respective characteristic variables and optimized solutions are depicted accordingly using look-tables.

The novelty of this work lies in the introduction of a new drive state classification approach based on an n-dimensional discrete description, whereby optimal axes' discretization and clustering of vehicle states has been considered to improve the accuracy of respective state-wise solutions. The analysis of results, considering different types of driving cycles, reveals the significant potential of proposed PMS to improve energy consumption at urban, highway and mixed-type driving cycles.

Further outlooks of this work include the development of state-predictive PMS based grid-space solutions and the assessment of computational requirements using real vehicular platforms.

References

[1] H. Zhang, C. J. R. Sheppard, T. E. Lipman, and S. J. Moura, "Joint fleet sizing and charging system planning for autonomous electric vehicles," *IEEE Transactions on Intelligent Transportation Systems*, vol. 21, no. 11, pp. 4725–4738, 2020.

[2] O. N. Nezamuddin, C. L. Nicholas, and E. C. d. Santos, "The problem of electric vehicle charging: State-of-the-art and an innovative solution," *IEEE Transactions on Intelligent Transportation Systems*, vol. 23, no. 5, pp. 4663–4673, 2022.

[3] L. Zhang, Z. Zeng, and X. Qu, "On the role of battery capacity fading mechanism in the lifecycle cost of electric bus fleet," *IEEE Transactions on Intelligent Transportation Systems*, vol. 22, no. 4, pp. 2371–2380, 2021.

[4] R. Deng, Y. Liu, W. Chen, and H. Liang, "A survey on electric buses—energy storage, power management, and charging scheduling," *IEEE Transactions on Intelligent Transportation Systems*, vol. 22, no. 1, pp. 9–22, 2021.

[5] A. M. Ali and B. Moulik, "On the role of intelligent power management strategies for electrified vehicles: A review of predictive and cognitive methods," *IEEE Transactions on Transportation Electrification*, vol. –, no. 2332-7782, pp. 1–16, Sep. 2021. [Online]. Available: https://doi.org/10.1109/TTE.2021.3115985

[6] J. Peng, H. He, and R. Xiong, "Rule based energy management strategy for a series–parallel plug-in hybrid electric bus optimized by dynamic programming," *Applied Energy*, vol. 185, pp. 1633–1643, jan 2017.

[7] S. Mehar, S. Zeadally, G. Remy, and S. M. Senouci, "Sustainable transportation management system for a fleet of electric vehicles," *IEEE Transactions on Intelligent Transportation Systems*, vol. 16, no. 3, pp. 1401–1414, Jun 2015.

[8] L. Guo, B. Gao, Y. Gao, and H. Chen, "Optimal energy management for hevs in eco-driving applications using bi-level MPC," *IEEE Transactions on Intelligent Transportation Systems*, vol. 18, no. 8, pp. 2153–2162, Aug. 2017.

[9] Y. Zou, Z. Kong, T. Liu, and D. Liu, "A real-time markov chain driver model for tracked vehicles and its validation: Its adaptability via stochastic dynamic programming," *IEEE Transactions on Vehicular Technology*, vol. 66, no. 5, pp. 3571–3582, May 2017.

[10] C. Sun, X. Hu, S. J. Moura, and F. Sun, "Velocity predictors for predictive energy management in hybrid electric vehicles," *IEEE Transactions on Control Systems Technology*, vol. 23, no. 3, pp. 1197–1204, May 2015.

[11] J. Nilsson, M. Brännström, E. Coelingh, and J. Fredriksson, "Lane change maneuvers for automated vehicles," *IEEE Transactions on Intelligent Transportation Systems*, vol. 18, no. 5, pp. 1087–1096, May 2017.

[12] G. Mahler and A. Vahidi, "An optimal velocity-planning scheme for vehicle energy efficiency through probabilistic

prediction of traffic-signal timing," *IEEE Transactions on Intelligent Transportation Systems*, vol. 15, no. 6, pp. 2516–2523, Dec. 2014.

[13] A. M. Ali, R. Shivapurkar, and D. Söffker, "Optimal situation-based power management and application to state predictive models for multi-source electric vehicles," *IEEE Transactions on Vehicular Technology*, vol. 68, no. 12, pp. 11 473–11 482, Dec. 2019. [Online]. Available: https://doi.org/10.1109%2Ftvt.2019.2948918

[14] B. Geng, J. K. Mills, and D. Sun, "Two-stage energy management control of fuel cell plug-in hybrid electric vehicles considering fuel cell longevity," *IEEE Transactions on Vehicular Technology*, vol. 61, no. 2, pp. 498–508, Feb. 2012.

[15] Q. Gong and J. Kapadia, "Customer data driven phev refuel distance modeling and estimation," in *SAE Technical Paper*. SAE International, Mar. 2017, pp. 1–7.

[16] X. Zeng and J. Wang, "A parallel hybrid electric vehicle energy management strategy using stochastic model predictive control with road grade preview," *IEEE Transactions on Control Systems Technology*, vol. 23, no. 6, pp. 2416–2423, Nov. 2015.

[17] Z. Chen, C. C. Mi, J. Xu, X. Gong, and C. You, "Energy management for a power-split plug-in hybrid electric vehicle based on dynamic programming and neural networks," *IEEE Transactions on Vehicular Technology*, vol. 63, no. 4, pp. 1567–1580, May 2014.

[18] M. Liebers, R. Kloß, and B. Bäker, "Combined power train and thermal management optimization using an extended dynamic programming," in *Proceedings*. Springer Fachmedien Wiesbaden, 2016, pp. 367–381.

[19] T. Liu, X. Tang, H. Wang, H. Yu, and X. Hu, "Adaptive hierarchical energy management design for a plug-in hybrid electric vehicle," *IEEE Transactions on Vehicular Technology*, vol. 68, pp. 11 513–11 522, 2019.

[20] P. Pisu and G. Rizzoni, "A comparative study of supervisory control strategies for hybrid electric vehicles," *IEEE Transactions on Control Systems Technology*, vol. 15, no. 3, pp. 506–518, may 2007.

[21] B. Moulik and D. Söffker, "Online power management with embedded offline-optimized parameters for a three-source hybrid powertrain with an experimental emulation application," *Energies*, vol. 9, no. 6, p. 439, jun 2016.

[22] J. Kessels, M. Koot, P. van den Bosch, and D. Kok, "Online energy management for hybrid electric vehicles," *IEEE Transactions on Vehicular Technology*, vol. 57, no. 6, pp. 3428–3440, nov 2008.

[23] S. Kermani, R. Trigui, S. Delprat, B. Jeanneret, and T. M. Guerra, "PHIL implementation of energy management optimization for a parallel HEV on a predefined route," *IEEE Transactions on Vehicular Technology*, vol. 60, no. 3, pp. 782–792, mar 2011.

[24] R. Wang and S. M. Lukic, "Review of driving conditions prediction and driving style recognition based control algorithms for hybrid electric vehicles," in *2011 IEEE Vehicle Power and Propulsion Conference*. IEEE, Sep. 2011.

[25] A. M. Ali and M. S. Asfoor, "Optimal battery sizing and stops allocation for electrified fleets using data-driven driving cycles: A case study for the city of cairo," *IEEE Transactions on Transportation Electrification*, pp. 1–1, 2022.

[26] E. Silvas, K. Hereijgers, H. Peng, T. Hofman, and M. Steinbuch, "Synthesis of realistic driving cycles with high accuracy and computational speed, including slope information," *IEEE Transactions on Vehicular Technology*, vol. 65, no. 6, pp. 4118–4128, Jun. 2016.

[27] J. Huertas, M. Giraldo, L. Quirama, and J. Díaz, "Driving cycles based on fuel consumption," *Energies*, vol. 11, no. 11, p. 3064, Nov. 2018.

[28] S. K. Mayakuntla and A. Verma, "A novel methodology for construction of driving cycles for indian cities," *Transportation Research Part D: Transport and Environment*, vol. 65, pp. 725–735, Dec. 2018.

[29] H. Kaymaz, H. Korkmaz, and H. Erdal, "Development of a driving cycle for istanbul bus rapid transit based on real-world data using stratified sampling method," *Transportation Research Part D: Transport and Environment*, vol. 75, pp. 123–135, Oct. 2019.

[30] A. M. Ali, A. Ghanbar, and D. Söffker, "Optimal control of multi-source electric vehicles in real time using advisory dynamic programming," *IEEE Transactions on Vehicular Technology*, vol. 68, no. 11, pp. 10 394–10 405, Nov. 2019.

[31] M. Zhao, H. Gao, Q. Han, J. Ge, W. Wang, and J. Qu, "Development of a driving cycle for Fuzhou using k-means and AMPSO," *Journal of Advanced Transportation*, vol. 2021, pp. 1–15, Feb. 2021.

[32] C. Fiori, V. Arcidiacono, G. Fontaras, M. Makridis, K. Mattas, V. Marzano, C. Thiel, and B. Ciuffo, "The effect of electrified mobility on the relationship between traffic conditions and energy consumption," *Transportation Research Part D: Transport and Environment*, vol. 67, pp. 275–290, Feb. 2019.

[33] C. M. Martinez, M. Heucke, F. Wang, B. Gao, and D. Cao, "Driving style recognition for intelligent vehicle control and advanced driver assistance: A survey," *IEEE Transactions on Intelligent Transportation Systems*, vol. 19, no. 3, pp. 666–676, March 2018.

[34] C.-K. Chau, K. Elbassioni, and C.-M. Tseng, "Drive mode optimization and path planning for plug-in hybrid electric vehicles," *IEEE Transactions on Intelligent Transportation Systems*, vol. 18, no. 12, pp. 3421–3432, 2017.

[35] R. Zhang, J. Tao, and H. Zhou, "Fuzzy optimal energy management for fuel cell and supercapacitor systems using neural network based driving pattern recognition," *IEEE Transactions on Fuzzy Systems*, p. 1, 2018.

[36] J. Shi, Y. Gao, W. Wang, N. Yu, and P. A. Ioannou, "Operating electric vehicle fleet for ride-hailing services with reinforcement learning," *IEEE Transactions on Intelligent Transportation Systems*, vol. 21, no. 11, pp. 4822–4834, 2020.

[37] D. Cui, Z. Wang, Z. Zhang, P. Liu, S. Wang, and D. G. Dorrell, "Driving event recognition of battery electric taxi based on big data analysis," *IEEE Transactions on Intelligent Transportation Systems*, pp. 1–10, 2021.

[38] M. Özbek, S. Wang, M. Marx, and D. Söffker, "Modeling and control of a PEM fuel cell system: A practical study based on experimental defined component behavior," *Journal of Process Control*, vol. 23, no. 3, pp. 282–293, mar 2013.

[39] J. Pukrushpan, A. Stefanopoulou, and H. Peng, "Modeling and control for pem fuel cell stack system," in *Proceedings of the 2002 American Control Conference (IEEE Cat. No.CH37301)*, vol. 4, 2002, pp. 3117–3122 vol.4.

[40] M. Özbek, S. Wang, M. Marx, and D. Söffker, "Modeling and control of a PEM fuel cell system: A practical study based on experimental defined component behavior," *Journal of Process Control*, vol. 23, no. 3, pp. 282–293, mar 2013.

[41] L. Gao, S. Liu, and R. Dougal, "Dynamic lithium-ion battery model for system simulation," *IEEE Transactions on Components and Packaging Technologies*, vol. 25, no. 3, pp. 495–505, Sep. 2002. [Online]. Available: https://doi.org/10.1109%2Ftcapt.2002.803653

[42] H. He, R. Xiong, X. Zhang, F. Sun, and J. Fan, "State-of-charge estimation of the lithium-ion battery using an adaptive extended kalman filter based on an improved thevenin model," *IEEE Transactions on Vehicular Technology*, vol. 60, no. 4, pp. 1461–1469, may 2011. [Online]. Available: https://doi.org/10.1109%2Ftvt.2011.2132812

[43] Q. Wang, Z. Wang, L. Zhang, P. Liu, and Z. Zhang, "A novel consistency evaluation method for series-connected battery systems based on real-world operation data," *IEEE Transactions on Transportation Electrification*, vol. 7, no. 2, pp. 437–451, 2021.

[44] X. Fan, W. Zhang, Z. Wang, F. An, H. Li, and J. Jiang, "Simplified battery pack modeling considering inconsistency and evolution of current distribution," *IEEE Transactions on Intelligent Transportation Systems*, vol. 22, no. 1, pp. 630–639, 2021.

[45] A. Farmann and D. U. Sauer, "Comparative study of reduced order equivalent circuit models for on-board state-of-available-power prediction of lithium-ion batteries in electric vehicles," *Applied Energy*, vol. 225, pp. 1102–1122, sep 2018.

[46] L. Zhang, Z. Wang, X. Hu, F. Sun, and D. G. Dorrell, "A comparative study of equivalent circuit models of ultracapacitors for electric vehicles," *Journal of Power Sources*, vol. 274, pp. 899–906, jan 2015. [Online]. Available: https://doi.org/10.1016%2Fj.jpowsour.2014.10.170

[47] N. Devillers, S. Jemei, M.-C. Péra, D. Bienaimé, and F. Gustin, "Review of characterization methods for supercapacitor modelling," *Journal of Power Sources*, vol. 246, pp. 596–608, jan 2014. [Online]. Available: https://doi.org/10.1016%2Fj.jpowsour.2013.07.116

[48] P. Sharma and T. Bhatti, "A review on electrochemical double-layer capacitors," *Energy Conversion and Management*, vol. 51, no. 12, pp. 2901–2912, dec 2010. [Online]. Available: https://doi.org/10.1016%2Fj.enconman.2010.06.031

[49] L. Helseth, "Modelling supercapacitors using a dynamic equivalent circuit with a distribution of relaxation times," *Journal of Energy Storage*, vol. 25, p. 100912, oct 2019.

[50] J. Bauman and M. Kazerani, "A comparative study of fuel-cell–battery, fuel-cell–ultracapacitor, and fuel-cell–battery–ultracapacitor vehicles," *IEEE Transactions on Vehicular Technology*, vol. 57, no. 2, pp. 760–769, mar 2008. [Online]. Available: https://doi.org/10.1109%2Ftvt.2007.906379

[51] D. Arthur and S. Vassilvitskii, "K-means++: The advantages of careful seeding," vol. 8, 01 2007, pp. 1027–1035.

[52] L. Kaufman and P. J. Rousseeuw, Eds., *Finding Groups in Data*. John Wiley & Sons, Inc., mar 1990. [Online]. Available: https://doi.org/10.1002%2F9780470316801

[53] A. M. Ali, R. Shivapurkar, and D. Söffker, "Development and improvement of a situation-based power management method for multi-source electric vehicles," in *2018 IEEE Vehicle Power and Propulsion Conference (VPPC)*. IEEE, Aug. 2018.

Ahmed M. Ali (M'21) received his B.Sc. and M.Sc. degrees, both in Automotive Engineering at the Military Technical College, Cairo, Egypt, in 2008 and 2015 respectively. He received his PhD (Dr.-Ing.) degree in Mechanical Engineering in 2019 at the University of Duisburg-Essen, Germany. He is now with the Automotive Engineering Department, The Military Technical College, Egypt. His fields of interest include optimal design and control of hybrid and electric powertrains, intelligent transportation systems, and fleets electrification.

Bedatri Moulik Bedatri Moulik received her Bachelors degree in Electrical Engineering and Masters degree in Control and Instrumentation Engineering from West Bengal University of Technology, Kolkata, India. She received her Dr.-Ing. Degree from the Chair of Dynamics and Control, University of Duisburg-Esssen, Germany. She is now an Assistant Professor at Amity University, Noida, India in the department of Electrical and Electronics Engineering

Dirk Söffker (M'10) received the Dr.-Ing. degree in mechanical engineering and the Habilitation degree in automatic control/safety engineering from University of Wuppertal, Wuppertal, Germany, in 1995 and 2001, respectively. Since 2001, he leads the Chair of Dynamics and Control with the Engineering Faculty, University of Duisburg-Essen, Germany. His current research interests include elastic mechanical structures, modern methods of control theory, human interaction with safety systems, safety and reliability control engineering of technical systems, and cognitive technical systems.